Estrogen-Induced Cell Cycle Arrest and Apoptosis as an Unexpected Outcome of Aromatase Inhibitor-Resistance in ER+ Breast Cancer

Hitomi Mori
City of Hope https://orcid.org/0000-0002-5416-5869
Kohei Saeki
City of Hope
Gregory Chang
City of Hope
Pei-Yin Hsu
City of Hope National Medical Center
Jinhui Wang
City of Hope
Xiwei Wu
City of Hope
Noriko Kanaya
City of Hope
Xiaoqiang Wang
City of Hope
George Somlo
City of Hope National Medical Center
Masafumi Nakamura
Kyushu University
Shiuan Chen (SChen@coh.org)
https://orcid.org/0000-0002-4482-6926

Research article

Keywords: Estrogen-induced apoptosis, Aromatase inhibitor resistance, Single cell RNA sequencing, Patient-derived tumor xenograft, Cell cycle arrest

Posted Date: February 24th, 2021

DOI: https://doi.org/10.21203/rs.3.rs-236742/v1

Abstract

Background: Estrogen is known to promotes hormone-dependent breast cancer through activation of estrogen receptor (ER)-α encoded by *ESR1*. However, several clinical trials reported the unexpected therapeutic benefit of E2 for aromatase inhibitor (AI)-resistant cases of ER^+ breast cancer. Considering potential impact of such clinical observation, we decided to determine the mechanisms of estrogen-induced tumor regression.

Methods: A unique estrogen-inhibitory patient-derived xenograft (PDX) tumor, GS3, was established from an AI resistant $ER^+/HER2^-$ brain metastatic breast cancer. *In vivo* estrogen suppression was confirmed through experiments by implanting 17β-estradiol (E2) pellets in mice carrying GS3, and then the single-cell analysis was performed using GS3 tumors. *In vitro* E2 suppression analysis was carried out using organoids from GS3.

Results: The E2-induced suppression of GS3 involves ERα, which was wild-type and not amplified. Single cell RNA sequencing analysis of this PDX has revealed that E2 treatment (for 1 week) induces cell cycle arrest in both $ESR1^+$ cells and $ESR1^-$ cells, demonstrating the unexpected influence of estrogen on $ESR1^-$ cells in ER^+ breast cancer. E2 upregulated the expression of estrogen-regulated genes, including a tumor suppressor gene, *IL24*, and lower levels of *IL24* were linked to estrogen independence, after three rounds of intermittent E2 treatment. $IL24^+$ cells included more G1 phase cells of cell cycle compared to $IL24^-$ cells. Hallmark apoptosis gene sets were upregulated and the hallmark G2M checkpoint gene set was downregulated in $IL24^+$ cells after E2 treatment. The number of apoptotic cells was significantly increased after long term (for 4 weeks) E2 treatment. Western blotting analysis demonstrated that long term E2 treatment induced expression of apoptosis-associated protein cleaved-PARP and reduction of the pro-survival protein Bcl-xl level.

Conclusions: There is the need of markers for patients who can benefit from E2 treatment after AI resistance, and measurements of ER and PR expression are not enough. Analysis of GS3 PDX has revealed that estrogen induces cell cycle arrest and apoptosis. Our study has revealed the cross-talk between $ESR1^+$ and $ESR1^-$ cells as well as potential roles of *IL24* in estrogen-suppressive tumors.

Background

Estrogen, such as 17β-estradiol (E2), plays a crucial role in the progression of hormone-dependent breast cancer through activation of estrogen receptor (ER). By suppressing estrogen production, aromatase inhibitors (AIs) are the first choice for $ER^+/HER2^-$ postmenopausal breast cancer [1–3], and they improve the outcomes of these patients [4–6]. Clinically, AI resistance is frequent [5]. Considering that AI resistant cancers develop their ability to grow without estrogen, important AI resistant cell lines were established from hormone-dependent breast cancer cell lines, such as MCF-7 and T-47D cells, through culture under long-term estrogen deprivation (LTED) [7–11]. Some of these LTED cell lines showed higher ER expression and estrogen hypersensitivity [10]. In some LTED cell lines, growth factor receptors and

downstream signaling pathways, including the MAPK, PI3K/AKT/mTOR, and JNK pathways, could function as an alternative growth signaling pathway, independent of ER [12]. Importantly, estrogen-dependent suppression of cell proliferation was reported after a long-term culture of LTED lines [13–18], suggesting that estrogen-induced tumor regression may be also an outcome of AI resistance. ER^+ cancer cell lines (LTED-MCF7), murine mammary adenocarcinomas (C7-2-HI, C4-HI), and one patient-derived xenograft (PDX) model (WHIM16) have been used to characterize the underlying therapeutic response mechanism of breast cancer to estrogen. Previous reports have indicated that the mechanism of E2-induced apoptosis includes *ESR1* amplification, endoplasmic reticulum stress [13–17] and/or the activation of the Fas/FasL pathway [18].

PDXs are superior to cell lines because they typically maintain the biological feature of original tumors and have proper multi-cellular architecture. We succeeded in establishing a unique AI-resistant PDX model named GS3 from an AI-resistant brain metastatic postmenopausal breast cancer. GS3 is not only an AI-resistant model, but also an estrogen-induced tumor regression model. Our GS3-PDX is a very important model because its AI resistance and E2 suppression were obtained clinically in the patient, rather than generated *in vitro*. The availability of GS3 offered us an unusual opportunity to assess how E2 induced tumor regression in AI-resistant ER^+ breast cancer. Our investigation reveals a new mechanism of estrogen-induced suppression that is different from those reported using other model systems. Considering the tumor heterogeneity, we performed single cell RNA sequencing (scRNAseq) to evaluate the gene expressions at the individual cell level and to compare the signaling pathways between cells, especially between *ESR1*$^+$ cells and *ESR1*$^-$ cells. These results indicate a novel concept of estrogen-induced apoptosis of breast cancer and identify the role of an estrogen-regulated tumor suppressor, *IL24*.

Methods

PDX

GS3, an estrogen-suppressive model, was established from an AI resistant brain metastatic postmenopausal breast cancer and whose subtype was ER^+ (100 %), PR^+ (5 %), and $HER2^-$. The diagnosis of the original tumor was stage III left breast cancer with left axillary and infraclavicular lymph node metastasis, and the patient received neoadjuvant chemotherapy (carboplatin and paclitaxel), surgery (left breast segmentectomy and axillary lymph node dissection), radiotherapy, and then continued with AI therapy. However, three years and nine months after surgery, brain metastasis was found. Surgically resected brain metastasis tumor pieces were implanted into the 4th mammary fat pat of 6–8 weeks old female NOD-scid/IL2R$\gamma^{-/-}$ (NSG) mice to establish the PDX lines. The details for PDX preparation were previously described [19].

In vivo **animal study**

Tumor pieces from an established GS3 were implanted into mammary fat pads of 8–10 weeks old female NSG mice. To confirm that GS3 is indeed resistant to AI, NSG mice bearing serially transplanted

GS3 were treated with placebo or letrozole (10 mg with 0.3% hydroxypropylcellulose in 0.9% NaCl solution, daily subcutaneous injection) [20] for 28 days. There was no difference in tumor growth rates and Ki-67 expression of immunohistochemistry (IHC) between placebo- and letrozole-treated GS3 (Fig. S1a, b), but letrozole treatment blocked the mouse mammary gland development. Cell viability assay also showed that organoids isolated from GS3 tumor were resistant to AI (Fig. S1c). After tumor volume reached approximately 200mm^3, mice were randomized and implanted with an E2 (1 mg) or placebo pellet on their backside. These treatments lasted 7 days for experiments on single cell analysis and lasted 5 days, 10 days, 28 days, and 53 days for bulk RNA sequencing (RNAseq) experiments. For intermittent E2 treatment, mice were implanted with the E2 (1 mg) pellet which remained in the mice 28 days, and then the pellet was removed on day 28. After 28 days interval with no treatment, the mice were again implanted with the E2 (1 mg) pellet for another 28 days. This intermittent E2 treatment was repeated three rounds. ICI (Fluvestrant, Astrazeneca, Cambridge, UK) was injected subcutaneously (5 mg in 100 µl sterile saline, once weekly) 4 times. Each treatment group of all animal experiments included at least three mice. Mice were randomized into each treatment group. All experiments were performed in replicate to confirm that the results we observed were statistically significant.

Histological analysis

IHC and Hematoxylin and eosin (H&E) staining of formalin-fixed tumor tissues were performed by the Pathology Core facility at City of Hope. Antibodies used in IHC included ERα (ab16660, Abcam, Cambridge, UK), PR (PA0312, Leica Biosystems Inc., Wetzlar, Germany), HER2 (A0485, Dako, Glostrup, Denmark), and Ki-67 (M7240, Dako, Glostrup, Denmark). ApopTag Plus Peroxidase *In Situ* Apoptosis Detection Kit (S7101, EMD Millipore Corporation, Burlington, MA) labeled apoptotic cells in formalin-fixed tumor tissue samples, identical to a TUNEL assay.

Western blotting

Total protein from the 7-day, 28-day, intermittent E2-treated and placebo-treated GS3 tumors were extracted using the Precellys Lysing Kit (Bertin Technologies, Montigny-Le-Bretonneux, France) and lysis buffer (50 mM Tris-HCl, 0.15 M NaCl, 1% Nonident P40, 0.5% sodium deoxycholate). After centrifuge at 15,000 × *g* for 30 min, the supernatants were collected for Western blotting analysis. Antibodies used in Western blotting included ERα (sc-8002, Santa Cruz Biotechnology, Santa Cruz, CA), poly (ADP-ribose) polymerase (PARP) and Cleaved-PARP (#9542, Cell Signaling Technology, Danvers, MA), Bcl-xL (#2764, Cell Signaling Technology, Danvers, MA), Bax (#2772, Cell Signaling Technology, Danvers, MA), GAPDH (#5174, Cell Signaling Technology, Danvers, MA).

Reverse phase protein array (RPPA) analysis

Each two snap-frozen tumor samples from the 5-day, 10-day, 53-day E2-treated and no treatment GS3 were subjected to RPPA analysis probed a total of 291 antibodies conducted by the MD Anderson Cancer Center Functional Proteomics RPPA Facility as described previously [21]. RPPA data of untreated GS3 samples were used as a reference.

Real-time PCR analysis

Total RNA for real-time PCR was extracted from GS3 tumors and organoids using the RNeasy Plus Mini Kit (Qiagen, Hilden, Germany). Reverse transcription reactions were performed with iScript RT reagent (BioRad, Hercules, CA) according to the manufacturer's instructions. Real-time PCR was performed with SYBER Green FastMix for Real-time PCR (Quantabio, Beverly, MA). The mRNA expression was normalized against both β-actin and GAPDH allowing comparison of mRNA levels. Primers used in this study are listed in Table S1.

Bulk RNAseq and analysis

Total RNA from GS3 tumors were extracted using the RNeasy Plus Mini Kit (Qiagen, Hilden, Germany) and then subjected to RNAseq conducted by the Integrative Genomics Core at the City of Hope. The first run included the 5-day, 10-day, 53-day E2-treated and no treatment samples. The second run included the 28-day and intermittent E2-treated, and placebo-treated samples. All RNA samples were extracted from two biological replicates. All sequencing data was submitted to the GEO database (GSE156922). Gene set enrichment analysis (GSEA) was performed using genes ranked by the fold changes between the different conditions to evaluate the significance activation of 50 HALLMARK gene sets in MSigDB22.

GS3 dissociation into single cell suspension

We isolated cells from the GS3 tumor in mice of two treatment groups: E2 (1 mg) and placebo. Cells isolated from two biological replicates were analyzed together. The GS3 tumors, of which total weight was 190 mg of E2-treated and 66.8 mg of placebo-treated, were cut into small, 2 mm thick strips and digested with 1.5 mg/mL DNAse I (#10104159001, Millipore Sigma, St. Louis, MO), 0.4 mg/mL Collagenase IV (CLS-4, Lot: 47E17528A, Worthington, Lakewood, NJ), 5% FBS, 10mM HEPES in HBSS. The mixture was strained through a 70 μm cell strainer. 1 mL of ACK lysis buffer was used to remove residual red blood cells from the sample. Dead cells were removed using Dead Cells Removal Microbeads (Miltenyi Biotec, Bergisch Gladbach, Germany).

ScRNAseq and analysis

Cell number and viability were measured using a TC20 Automated Cell Counter (BioRad, Hercules, CA). We only processed samples that showed at least 80% viability. Cells were then loaded onto the Chromium Controller (10x Genomics, Pleasanton, CA) targeting 2,000–5,000 cells per lane. The Chromium v2 single cell 3' RNA-seq reagent kit (10x Genomics, Pleasanton, CA) was used to process samples into scRNA-seq libraries according to the manufacturer's protocol. Libraries were sequenced with a Hiseq 2500 instrument (Illumina, San Diego, CA) with a depth of 50k–100k reads per cell. Raw sequencing data were processed using the 10x Genomics Cell Ranger pipeline (version 2.0) to generate FASTQ files and aligned to mm10 genome to gene expression count. All sequencing data was submitted to the GEO database (GSE156752). The subsequent data analysis was performed using the Seurat package and R software unless otherwise specified. Cells with mitochondrial read rate > 20% and < 200 detectable genes were considered as low-quality and filtered out. After normalization and scaling, cell cycle prediction was

performed using the *CellCycleScoring* function and gene expression heterogeneity due to cell cycle was regressed out [22]. Then, the data was clustered using the top principal components of highly variable genes (HVGs). A uniform manifold approximation and projection (UMAP) was used to visualize the resulting clusters. Cluster-specific markers were identified to generate heatmap and feature plots in the identified cell clusters. Trajectory analysis was performed using the Monocle package and R software. GSEA analysis was also performed on the single cell level, using genes ranked by mean centered log2-normalized read counts and Hallmark gene sets in MSigDB.

Organoids and in vitro **treatment study**

Estrogen-suppressive organoids were established from fresh surgical specimens of GS3 using 3D culture conditions (Fig. S2). After tumor tissue was minced and digested, 10^4 of organoids were embedded in VitroGel 3D-RGD (TWG002, TheWell Bioscience, North Brunswick, NJ) on a 96 well plate and cultured in E2-free M87 medium at 37˚C [23]. The organoids viability was evaluated using the CellTider-Glo 3D Cell Viability Assay (G9682, Promega, Madison, WI) which measured ATP. We made at least five technical replicates and repeat experiments twice.

Statistics

To assess statistical significance, values of treated groups were compared to those of control/placebo groups by either two-way ANOVA or Student t-test, using GraphPad Prism 8 (GraphPad software, San Diego, CA). Error bars represent SEM. *P*-value of less than 0.05 was considered statistically significant.

Results

E2 treatment inhibited the proliferation of GS3 in vivo **and** in vitro

A consistent regression of GS3 was observed by the treatment of tumor-implanted mice with E2 (1 mg) for 28 days (Fig. 1a). This phenotype was preserved across serially transplanted GS3 tumors (up to 14 passages so far). GS3 tumor pieces that were simultaneously transplanted with E2, showed no growth for half a year; meanwhile GS3 tumor pieces implanted alongside a placebo pellet (no E2) grew beyond 1000 mm^3 (Fig. 1b). A repeating pattern of regression and growth of the GS3 tumor volume was observed when subjected to intermittent E2 treatment. After three rounds of intermittent E2 treatment on GS3, an E2 independent growth developed (Fig. 1c). To examine the effect of E2 on the proliferation of GS3 *in vitro*, organoids were generated from untreated GS3 tumors. E2 suppressed the proliferation of GS3 organoids in an E2 concentration-dependent manner (Fig. 1d).

E2 downregulated the expression of ERα and cell cycle proliferation genes in GS3

ERα and ERβ genes in GS3 were wild-type and not amplified. The only other reported estrogen-suppressive PDX, WHIM16, has an *ESR1* amplification [17, 24]. To determine which ER subtype is involved in E2-induced regression of GS3, we performed co-treatment of E2 and ERα-specific antagonist (MPP) or ERβ-specific antagonist (PHTPP) *in vitro*. E2-mediated inhibition of GS3-organoids could be

reversed by the co-treatment of MPP, but not by PHTPP (Fig. 2a), indicating the participation of ERα in this suppression process. H&E staining showed that cell density (the number of cells per square) decreased after E2 treatment (Fig. 2b). IHC indicated that the proportion of $ERα^+$ cells decreased, and ERα staining intensity was reduced after E2 treatment depending on treatment terms (Fig. 2b). Western blotting and RPPA analysis showed that the E2 treatment resulted in lower ERα protein level *in vivo* (Fig. 2c, d). E2 treatment decreased the *ESR1* expression of GS3-organoids at the mRNA level *in vitro* as well (Fig. 2e). IHC also showed that progesterone receptor (PR) $^+$ cells appeared in E2-treated tumors (Fig. 2b) and that E2 treatment increased the levels of PR protein and of mRNA (Fig. 2d, e, respectively). However, the number of Ki-67^+ cells in IHC (Fig. 2b) and the CDK1 and cyclin-B1 expressions at the protein level in RPPA (Fig. 2d) decreased after E2 treatment.

To investigate the overall effects of E2 treatment on GS3, bulk RNAseq was performed using 5-, 10-, and 53-day E2-treated tumors as well as control tumors. GSEA analysis showed that the hallmark estrogen response early/late gene sets were upregulated after E2 treatment (Table S2). Although the *ESR1* expression level decreased (possibly in part due to reduction of $ERα^+$ cells, as indicated by IHC), expression levels of ER target genes, such as *PGR*, *GREB1*, and *TFF1*, increased depending on the E2 treatment time (Fig. 2f). In addition, cell cycle progression genes, such as *CDK1*, *TOP2A, E2F2*, and *MKI67*, were down-regulated in E2-treated tumors (Fig. 2f). The organoids isolated from longer E2-treated tumors expressed a higher level of ER target genes (Fig. 2g). In addition, the expression of two tumor suppressor genes, *IL24* and *GADD45A*, was upregulated in E2-treated PDXs, as well as in organoids that were isolated from E2-treated tumors, depending on treatment time (Fig. 2f, g). Collectively, our examination of GS3 tumors after E2 treatment indicates that inhibition of GS3 growth is associated with a reduction of $ERα^+$ cells, an increased expression of ERα target genes (as an indication of the presence of functional active ERα), and an induced cell cycle arrest and growth suppression.

scRNAseq to study effects of E2 on GS3

To better understand the mechanism of estrogen-induced growth suppression and the potential contributions of $ERα^+$ cells and $ERα^-$ cells, we performed scRNAsEq. Following a treatment which lasted 7 days using E2 (1 mg) or a placebo pellet, GS3 tumors were harvested and digested into a single cell suspension. Although results of longer E2/placebo treatments showed larger differences of gene expressions according to the bulk RNAseq analysis, the viability of single cells isolated from GS3 tumors decreased after the tumors shrunk. Since the presence of a large number of dead cells would affect the quality of single cell analysis, we decided to treat GS3-PDX for 7 days in which the single cells' viability was more than 80%. Single cell samples were prepared for scRNAseq using a 10x Genomics platform. Single cell preparations from two tumors from each treatment were combined and processed for scRNAseq (Fig. 3a). After filtering out mouse-derived cells (8% of total cells) based on their species-specific sequences, 20,467 genes were detected from 10,631 cells: 3,927 cells from placebo-treated tumors and 6,704 cells from E2-treated tumors. These were all epithelial cells that expressed human genes. The principle component analysis was performed on 2,000 HVGs. A UMAP was generated to

summarize and visualize the data in a two-dimensional subspace, which led to the identification of 4 major cell clusters (C0–C3) in GS3 (Fig. 3b), where each dot represented one cell. The number of cells in each cluster is specified in Table S3.

Characteristics of 4 single cell clusters

The relationships between 4 clusters were visualized by a heat map using the top 20 differentially expressed genes (DEGs) and hierarchical clustering based on the average expression of HVGs (Fig. 3c, d). Top 20 DEGs in C0 and C1 included commonly known ER target genes. Those top 20 DEGs in C2 included genes of the hallmark TNFA signaling via NFKB gene set, and those in C3 included cell cycle progression genes. Although cells with a mitochondrial read rate > 20% were already excluded, C0 and C2 included cells with higher expression of mitochondrial genes (Fig. 3c). The gene expression pattern of C0 was relatively similar to that of C2, while C1 was similar to C3 (Fig. 3d). GSEA analysis of each cluster indicated that there were three important hallmark gene sets in GS3: the hallmark estrogen response early/late and G2M checkpoint (Table S4). The hallmark estrogen response early/late gene sets were upregulated in C0 and downregulated in C3. In contrast, the hallmark G2M checkpoint gene set was significantly downregulated in C0 and upregulated in C3 (Table S4).

Impact of E2 on gene expression at the single-cell level

Cells from E2- or placebo-treated tumors were clearly placed in different clusters (Fig. 3e). More than 90% of the cells in C0 and C1 were E2-treated cells and more than 95% of the cells in C2 and C3 were placebo-treated cells (Fig. S3a). The cell cycle scoring was performed using the Seurat package according to the developer's vignette. C0/C2 included more G1 phase cells while C1/C3 included more G2M phase cells (Fig. 3f, Fig. S3b). GSEA analysis of the direct comparison between C0 and C2 showed that the hallmark estrogen response early/late gene sets were upregulated in C0, where most of the cells were from E2-treated tumors. Comparing C1 to C3 directly, the hallmark G2M checkpoint was downregulated in C1, where the majority of the cells were also from E2-treated tumors. The hallmark estrogen response early/late gene sets were upregulated in C1 compared to C3 as well (Table S4).

Comparison of E2-treated cells vs. placebo-treated cells

Most *ESR1*$^{+}$ cells were distributed between C0 and C2 (Fig. 4a). The percentage of *ESR1*$^{+}$ cells decreased by 10% in E2-treated cells compared to placebo-treated cells. However, the percentage of cells expressing ER target genes, such as *PGR*, *PDZK1*, *SERPINA1*, and *GREB1*, dramatically increased in E2-treated cells (Fig. 4a). Furthermore, the percentage of cells expressing cell cycle progression genes, such as *MKI67*, *CCNE2*, *CCNA2*, and *E2F2*, decreased in E2-treated cells (Fig. 4b). Distribution of cells remaining at the G1, S, or G2M phase in GS3 changed after 7 days of E2 treatment. The percentage of cells which progressed to the G2M phase decreased (-4.7%) and the percentage of cells that arrested at the G1 phase increased (+ 12.5%) in E2-treated cells (Fig. 4c).

Crosstalk between ESR1^{+} cells and ESR1^{-} cells

The percentage of cells which were arrested at the G1 phase increased by 10.9% in *ESR1*$^{+}$ cells and by 16.0% in *ESR1*$^{-}$ cells after E2 treatment. In addition, the percentage of cells progressing to the G2M phase decreased by 3.4% and 7.8% in *ESR1*$^{+}$ and *ESR1*$^{-}$ cells respectively. The decreasing of G2M phase cells after E2 treatment was greater in *ESR1*$^{-}$ cells compared to *ESR1*$^{+}$ cells (Fig. 4d). To clarify the difference of signaling pathways between *ESR1*$^{+}$ cells and *ESR1*$^{-}$ cells, we performed GSEA analysis for *ESR1*$^{+}$ cells and *ESR1*$^{-}$ cells separately. Interestingly, the hallmark estrogen response early/late gene sets were upregulated not only in *ESR1*$^{+}$ cells, but also in *ESR1*$^{-}$ cells after E2 treatment. Moreover, the hallmark G2M checkpoint gene set was significantly downregulated in *ESR1*$^{-}$ cells after E2 treatment (Table 1). Therefore, our single cell analysis revealed that E2 treatment upregulated the expression of estrogen response genes and reduced the proliferation of both *ESR1*$^{+}$ and *ESR1*$^{-}$ cells in GS3.

Table 1

Hallmark gene sets analysis of *ESR1*$^{+}$ cells and *ESR1*$^{-}$ cells

	Upregulated in E2 (vs. placebo)	***P*-value**	**Downregulated in E2 (vs. placebo)**	***P*-value**
ESR1^{-} **cells**	**ESTROGEN_RESPONSE_LATE**	1.22E-16	**G2M_CHECKPOINT**	1.45E-30
	ESTROGEN_RESPONSE_EARLY	2.99E-15	E2F_TARGETS	2.83E-22
	HTNFA_SIGNALING_VIA_NFKB	1.06E-07	TNFA_SIGNALING_VIA_NFKB	1.74E-12
ESR1^{+} **cells**	**ESTROGEN_RESPONSE_EARLY**	2.69E-19	TNFA_SIGNALING_VIA_NFKB	1.59E-20
	ESTROGEN_RESPONSE_LATE	7.36E-18	P53_PATHWAY	7.78E-13
	ANDROGEN_RESPONSE	5.45E-05	APOPTOSIS	1.07E-11

E2-induced IL24^{+} **cells through ERα**

The percentage of *IL24*$^{+}$ cells in the E2-treated was 2.75-fold of that in placebo-treated cells (Fig. 5a). *IL24*$^{+}$ cells included more *ESR1*$^{+}$ cells compared to *IL24*$^{-}$ cells. In *IL24*$^{+}$ cells, the percentage of cells that progressed to the G2M phase decreased (-12.4%) and those that arrested at the G1 phase increased (+ 9.7%) when compared to those in the *IL24*$^{-}$ cells (Fig. 5b). *IL24*$^{+}$ cells expressed higher levels of mitochondrial genes than *IL24*$^{-}$ cells (Fig. 5c). When comparing *IL24* expression levels in total mRNA extracted from GS3 tumors, *IL24* expression level was upregulated after E2 treatment in a time dependent manner and its expression was inhibited by ICI (Fig. 5d).

The GS3 tumors obtained E2 independence after the three rounds of intermittent E2 treatment. The decrease of ERα^{+} cells and Ki-67^{+} cells after E2 treatment was reversed after intermittent E2 treatment

(Fig. 2b). To identify the key pathway driving E2 independence, we performed bulk RNAseq on GS3 tumors treated with placebo, E2 (for 28 days), or intermittent E2. The hierarchical clustering using 1,312 DEGs showed that approximately 60% of genes in the intermittent E2-treated sample had the same trend as E2-treated samples (mainly ER target genes), in which 40% of the genes behaved similarly to the placebo-treated sample (mainly cell cycle progression genes) (Fig. 5e). The *IL24* expression level was upregulated in E2-treated tumors when compared to placebo-treated tumors and downregulated in intermittent E2-treated tumors when compared to (continuous) E2-treated tumors (Fig. 5d).

To clarify the difference of signaling pathways between *IL24*$^-$ cells and *IL24*$^+$ cells, we performed GSEA analysis for *IL24*$^-$ cells and *IL24*$^+$ cells separately. The hallmark TNFA signaling via NFKB, hallmark estrogen response early/late, and hallmark apoptosis gene sets were upregulated in *IL24*$^+$ cells after E2 treatment. On the other hand, the hallmark G2M checkpoint gene set was downregulated in *IL24*$^+$ cells after E2 treatment (Table 2).

Table 2

GSEA hallmark gene sets analysis of genes expressed on *IL24*$^+$ cells vs. *IL24*$^-$ cells

Upregulated in *IL24*$^+$ cells	*P*-value	Downregulated in *IL24*$^+$ cells	*P*-value
TNFA_SIGNALING_VIA_NFKB	1.06E-37	**G2M_CHECKPOINT**	1.05E-08
ESTROGEN_RESPONSE_LATE	7.60E-12	E2F_TARGETS	1.05E-08
ESTROGEN_RESPONSE_EARLY	4.46E-10	MYC_TARGETS_V1	6.05E-05
APOPTOSIS	6.03E-09	P53_PATHWAY	2.71E-03

Predication of the transitions between placebo-treated cells and E2-treated cells by trajectory analysis

To investigate the transition between placebo-treated cells and E2-treated cells, single cell trajectory analysis was performed using Monocle, an algorithm that explores relationships between cells through pseudo-time. There were 12 different ‘cell states’ identified during the trajectory analysis (Fig. 6a). The number of cells and distribution of cells treated with E2/placebo in each state are in Table S5 and Fig. S4a. The trajectory colored by four clusters in the UMAP (Fig. 3b) was shown in Fig. S4b. Trajectory analysis of single cells revealed three major branches associated with [I] placebo (State 1–2), [II] E2 (State 3–11), and [III] common E2 and placebo (State 12) (Fig. 6b). In the E2 branched group, *ESR1*$^+$ cells and G1 phase cells progressively decreased from state 9 (the endpoint of the E2 branch) to state 3 (junction), and G2M phase cells increased inversely with *ESR1*$^+$ cells and G1 phase cells (Fig. 6c, d). The hallmark estrogen response early/late gene sets were upregulated in both *ESR1*$^+$ cells and *ESR1*$^-$ cells (Fig. 6e). Significantly, the hallmark G2M checkpoint gene set was downregulated, even in *ESR1*$^-$ cells (Fig. 6e). *IL24*$^+$ cells and *PGR*$^+$ cells were primarily distributed in state 9, which was the endpoint of the E2 branched group (Fig. 6f, Fig. S4c). There were very few *IL24*$^+$ cells within state 9 at the G2M phase (Fig. 6g). As expected, in the placebo branched group, the hallmark estrogen response early/late gene sets were not upregulated, and the hallmark G2M checkpoint gene set was not downregulated in *ESR1*$^+$

cells, when compared to the E2 branched group (Fig. 6e). In the common branch (containing cells from both placebo- and E2-treated tumors) that included both *ESR1*$^{+}$ cells and *ESR1*$^{-}$ cells, there were no G1 phase cells and the hallmark G2M checkpoint was dramatically upregulated(Fig. 6e). *MKI67*$^{+}$ cells (at G2M phase), including some *ESR1*$^{+}$ cells, were mainly present in the placebo branch (State 1) and the common E2 and placebo branch (State 12) (Fig. S4c).

E2-induced apoptosis after the long-term E2 treatment

To investigate the relationship between tumor shrinkage and apoptosis, we detected apoptotic cells from formalin-fixed tumor tissues. A few apoptotic cells were observed in 28-day E2-treated tissue (Fig. 7a). There was a significant difference between placebo and 28-day E2-treated tissues ($P < 0.0001$, Fig. 7b). Western blotting analysis further demonstrated that long term (28-day) E2 treatment induced expression of apoptosis-associated proteins, as indicated by elevated levels of cleaved PARP (a hall mark of apoptosis) and the pro-apoptotic protein Bax, as well as by reduced levels of the pro-survival protein Bcl-xl. Cleaved-PARP expression was reduced after GS3 tumors gained E2 independence. (Fig. 7c).

Discussion

Using LTED cell models, estrogen-induced apoptosis has been proposed to be an outcome of AI resistance [13–18]. Examining the AI-resistant GS3 through scRNAseq analysis, we obtained valuable information regarding E2-suppressive mechanism in a patient-derived tumor.

E2 suppressed the growth of GS3 persevered after serial transplantations. AI resistance in our GS3 tumor was not caused by *ESR1* mutation, which was suggested as the driving factor by other investigators in their respective tumor models [25, 26]. GS3-PDX is also inherently different from the WHIM16-PDX model, which harbors the *ESR1* amplification as reported in previous studies [17, 24]. The exact mechanism of estrogen-mediated suppression of WHIM16-PDX has not yet been reported. We identified that ERα is involved in the E2-induced suppression of GS3 organoids (Fig. 2a). AI-resistance tumors often retain ER expression and ER signaling [27]. ScRNAseq can identify the differences among thousands of gene expression levels in individual cells. This advantage enables us to assign each individual cell to G1, S, or G2M phase, or to compare cells with/without a specific gene expression. While E2 increased the expression of ERα-regulated genes in GS3, E2 reduced the percentage of *ESR1*$^{+}$ cells, cells expressing cell cycle proliferation genes, and cells in the G2M phase (Fig. 4a–c). This is different from most ER^{+} breast cancers in that E2 increases ER level, expression of ER target genes (induced by ER), and promote proliferation [28, 29].

Our scRNAseq analysis of GS3 offered an opportunity to address the molecular and functional differences between *ESR1*$^{+}$ and *ESR1*$^{-}$ cells in ER^{+} tumors. After analyzing DEGs on *ESR1*$^{+}$ and *ESR1*$^{-}$ cells separately, the cell cycle proliferation gene set was downregulated mainly in *ESR1*$^{-}$ cells, and the E2

response gene sets were upregulated in not only *ESR1*$^+$ cells, but also *ESR1*$^-$ cells. While E2 should activate ERα and regulate *ESR1*$^+$ cells, our findings regarding *ESR1*$^-$ cells were unexpected and suggested crosstalk between *ESR1*$^+$ cells and *ESR1*$^-$ cells. While the detailed mechanisms of the crosstalk are yet to be better defined, this finding offers an important explanation as to why most of the estrogen-responsive breast cancers are not homogenously 100% ER$^+$.

Importantly, the results of bulk RNAseq of GS3 tumors revealed that the *IL24* expression level increased remarkably after E2 treatment in a time dependent manner (Fig. 2f); we confirmed that *IL24* was upregulated by ERα in GS3 (Fig. 5d). *IL24* was not included in the hallmark estrogen response early/late gene sets, but it has been documented that *IL24* was upregulated by E2 preferentially through ERα [30]. Interleukin-24 (IL-24) is a tumor suppressor cytokine that selectively induces apoptosis in a wide variety of human cancer cells, including breast cancer [31, 32]. *IL24*$^+$ cells were arrested in the G1 phase of the cell cycle (Fig. 5b), downregulating the hallmark G2M checkpoint gene set and upregulating the hallmark apoptosis gene set (Table 2). These results were consistent for IL-24 as a tumor suppressor. Publicly available data showing that high expression of IL-24 at the protein level is related to longer overall survival in breast cancer patients also further supported our results ($P = 0.00051$, Fig. S5). *IL24*$^+$ cells also included more mitochondrial genes compared to *IL24*$^-$ cells (Fig. 5c). Mitochondrial gene percentage was high in G1 phase cells and low in G2M phase cells (Fig. S6a). Mitochondrial gene percentage was also high in *ESR1*$^+$ cells and *PGR*$^+$ cells; in contrast, it was low in *MKI67*$^+$ cells, *CCNE2*$^+$ cells, and *CCNA2*$^+$ cells (Fig. S6b). Mitochondrial gene percentage could be an indicator of cell cycle arrest in GS3. Mitochondrial levels determine variability in cell death by modulating apoptotic gene expression [33]. Our analysis has revealed that TNFA Signaling via NFKB gene set has a strong association with *IL24*$^+$ cells. While the NFKB pathway has been linked to endocrine therapy resistance [34], the roles of this pathway in GS3 has not yet clearly defined.

Trajectory analysis reflected the notion of pseudo-time in the transition from placebo-treated cells to E2-treated cells. States 3–11 belonged to the E2-treated branch, and states 3–6 (junction side) were similar to the placebo branch (State 1 and 2) in regard to the cell cycle phase. On the other hand, states 7–11 (end side of the E2 branch) had E2 branch-specific features, such as a high number of G1 phase cells, a low number of G2M phase cells (Fig. 6c), upregulation of the estrogen response gene sets in *ESR1*$^+$ cells, and downregulation of the cell cycle proliferation gene set, especially in *ESR1*$^-$ cells (Fig. 6e). State 9 was the endpoint of the E2-treated branch. State 9 included the highest percentage of G1 phase cells and the lowest percentage of G2M phase cells compared to the other states (Fig. 6c). State 9 also included the highest percentage of cells expressing ER target genes. We considered that the GS3 cells gradually changed from state 3 to state 9 under the influence of E2. This would support the notion that *IL24*$^+$ cells, which were primarily distributed in state 9, are important for E2-induced tumor suppression. State 12 was the common E2- and placebo-treated branch. It included *ESR1*$^+$ cells as well (Fig. 6d). State 12 was quite different from the other states because it included 80% of the G2M phase cells and almost no G1 phase cells (Fig. 6c, Fig. S4a). Our results suggested that cells in state 12 were estrogen independent (Fig. 6e).

Intermittent E2 treatment tumor serves as a good reference control because GS3, intermittently treated with E2, was originally E2 dependent, but then became E2 independent. Since intermittent E2 treatment was performed every 28 days (E2 pellet on/off every 28 days, three times), we compared the placebo treatment for 28 days, E2 treatment for 28 days, and intermittent E2 treatment. After E2 treatment for 28 days, the hallmark estrogen response late gene set was upregulated and the hallmark G2M checkpoint gene set was downregulated: the same results as the short-term E2 treatment (Fig. S7a). Interestingly, the hallmark Reactive Oxygen Species (ROS) pathway gene set was upregulated after the long-term E2 treatment, despite the effective pathway size being relatively small (Fig. S7a). Upregulation of *IL24* expression level and the hallmark ROS pathway in 28-day E2 was reversed in intermittent E2 samples (Fig. 5d, Fig. S7b). Downregulation of the hallmark G2M checkpoint gene set in 28-day E2 was also reversed in intermittent E2 samples (Fig. S7b). These results support that *IL24* and the ROS pathway may play an important role in the cell cycle arrest induced by E2. ROS has double-faced role in cancer. High levels of ROS, resulting from abnormal cellular metabolism and inflammation, promote tumor proliferation, vascularization, and metastasis, while an excessive amount of ROS is likely to induce apoptosis. Mitochondrial dysfunction and ROS accumulation are important proapoptotic events occurring in cancer cells [35] [36]. There is accumulating evidence that the anti-cancer activity of IL-24 is primarily through the endoplasmic reticulum stress pathway, but other pathways leading to cell death are also exploited by IL-24 [37]. Production of ROS has been linked to endoplasmic reticulum stress [38] and IL-24-induced apoptosis [39]. A long-term (28-day) E2 treatment increased the level of apoptotic cells in GS3, and cleaved PARP was detected by Western blotting. On the other hand, cleaved PARP was not observed in the short-term (7-day) treatment (Fig. 7a–c). Thus, the results of single cell analysis (7-day E2 treatment) reflected the change of cells before apoptosis. As a result of *IL24* induced by E2 in GS3, the ROS pathway might be upregulated, and then the apoptotic pathway was activated (Fig. 8).

Estrogen-induced cell cycle arrest, in GS3 as well as in other reported cell culture models, can be an unexpected outcome of AI resistance, suggesting an estrogen therapy for such patients. In ER^+ breast cancer, estrogen is typically considered to promote the tumor growth. Therefore, clinicians hesitate to use E2 as a general treatment option for recurrent ER^+ tumors even when tumors are completely resistant to AI. Our mechanistic studies of GS3 offer leads into identifying such tumors that can respond to E2 therapies. The efficacy of the estrogen therapy for advanced breast cancer was first reported by Haddow et al in 1944 [40]. In the 1970s, randomized trials comparing estrogens versus tamoxifen in postmenopausal women with advanced breast cancer showed similar regression rates, with less toxicity using tamoxifen [41–43]. After 2001, several small-scale prospective clinical trials reported a therapeutic benefit with the different estrogens for AI-resistant cases of ER^+ postmenopausal breast cancer [44–49]. The clinical benefit rate of estrogen therapies is 26–56% in 7 trials (Table S6). Our findings point out that measurements of ER and PR expression alone are not sufficient to propose an E2 therapy. We need to identify the appropriate biomarkers to select patients who will benefit from undergoing E2 therapy. Our study has shown that IL24 could be a biomarker candidate for E2-induced suppression in AI-resistant ER^+ postmenopausal breast cancer.

We recognize several limitations in this study. It is a technical limitation to isolate 100% of living cells after tumor digestion for single cell analysis. We determined that the cell viability was around 80% in each sample for the 7-day treatment, significantly better than longer E2 exposure. Furthermore, we observed the difference between the ERα positivity rate of placebo-treated GS3 at the protein level by IHC and the *ESR1* positivity rate at mRNA level (100% in IHC and 41% in scRNAseq, respectively). The single cell isolation for solid tissue remains empirical. It is likely that different types of cells are fractionated with different efficiency. The other limitation is that our results were generated from a single PDX. There are only two estrogen-suppressive PDXs so far, GS3 and WHIM16. We consider GS3 as a valuable tumor model derived from a patient that reveals a new mechanism of estrogen-induced apoptosis, indicating more than one way for estrogen-induced suppression of breast cancer. With this in mind, additional estrogen-suppressive tumor specimens will be needed to verify these mechanisms.

Conclusions

E2-induced suppression is an unexpected outcome of AI resistance. In these cases, elimination of estrogen by AI results in maintaining tumor growth. Analysis of GS3-PDX has revealed that estrogen can induce cell cycle arrest and the expression of estrogen-regulated genes. As a conceptual advancement, our results also suggest crosstalk between *ESR1*$^{+}$ and *ESR1*$^{-}$ cells in ER^{+} tumors as well as potential roles of *IL24* that expresses in some breast cancer. Our findings point to the need for markers for such patients who can benefit from E2 treatment after AI resistance and whose measurements of ER and PR expression are not enough. Expression of *IL24* in AI-resistant tumors might be an indicator for response to E2 therapy. While E2-mediated suppression of GS3 has sustained throughout 14 passages so far, an intermittent treatment strategy would eliminate this estrogen-induced mechanism.

Abbreviations

E2: 17β-estradiol; ER: estrogen receptor; Ais: aromatase inhibitors; LTED: long-term estrogen deprivation; PDX: patient-derived xenograft; scRNAseq: single cell RNA sequencing; NSG: NOD-scid/IL2Rγ$^{-/-}$; IHC: immunohistochemistry; RNAseq: RNA sequencing; PARP: poly (ADP-ribose) polymerase; RPPA: Reverse phase protein array; GSEA: Gene set enrichment analysis; HVGs: highly variable genes; UMAP: uniform manifold approximation and projection; PR: progesterone receptor; DEGs: differentially expressed genes; IL-24: Interleukin-24; ROS: Reactive Oxygen Species

Declarations

Ethics approval and consent to participate

This study was approved by City of Hope Institutional Review Board and the patient provided written informed consent prior to tissue collection (IRB # 17030). All animal research procedures used in this study were approved by the Institutional Animal Care and Used Committee at city of Hope (IACUC

#91051). Facilities are created by Association for Assessment and Accreditation of Laboratory Animal Core and operated according to National Institutes of Health guideline.

Consent for publication

Not applicable

Availability of data and materials

The raw bulk RNAseq and scRNAseq data generated in this study has been deposited in GEO with the accession code GSE156922 (bulk RNAseq) and GSE156752 (scRNAseq).

https://www.ncbi.nlm.nih.gov/geo/query/acc.cgi?acc=GSE156922

https://www.ncbi.nlm.nih.gov/geo/query/acc.cgi?acc=GSE156752

Competing interests

All authors declare no conflicts of interest.

Funding

HM was supported in part by a Research Fellowship for Young Scientists from Japan Society for the Promotion of Science (JSPS KAKENHI JP18J20301). This work was supported by the Lester M. and Irene C. Finkelstein endowment, NIH U01ES026137, and a pilot grant from the City of Hope Center for Cancer and Aging.

Authors' contributions

S.C. and H.M. designed the study; H.M., G.C., P.Y.H, N.K. and X.W. (Xiaoqiang Wang) performed the experiments; J.W. performed the 10X library production and sequencing; H.M., K.S., G.C., and X.W. (Xiwei Wu) analyzed the data; G.S. provided the clinical sample; H.M. and S.C. wrote the paper; M.N. is responsible person of Funding acquisition (JSPS KAKENHI JP18J20301); S.C. supervised the research.

Acknowledgements

HM received a SABCS Basic Science Scholar Award supported by the 43rd San Antonio Breast Cancer Symposium, 2020, for her presentation on this research. We thank the City of Hope Integrative Genomics Core, Pathology Research Service Core, and Animal Resource Core, which are supported by the National Cancer Institute of the National Institutes of Health under award number P30CA033572, for the excellent technical support. We appreciate the assistance of Min-Hsuan and Charles Warden for processing bulk RNAseq and scRNAseq data. In addition, we thank Desiree Ha for editing our manuscript.

References

1. Chlebowski R, Cuzick J, Amakye D, Bauerfeind I, Buzdar A, Chiaf S, Cutulig B, Linforthh R, Maassi N, Noguchij S, et al. Clinical perspectives on the utility of aromatase inhibitors for the adjuvant treatment of breast cancer. The Breast. 2009;18:1–11.
2. Chumsri S, Howes T, Bao T, Sabnis G, Brodie A. Aromatase, aromatase inhibitors, and breast cancer. The Journal of Steroid Biochemistry Molecular Biology. 2011;125:13–22.
3. Lao Romera J, Puertolas Hernandez TJ, Pelaez Fernandez I, Sampedro Gimeno T, Fernandez Martinez R, Fernandez Perez I, Iranzo Gonzalez Cruz V, Illarramendi Manas JJ, Garcera Juan S, Ciruelos Gil EM. Update on adjuvant hormonal treatment of early breast cancer. Advances in Therapy. 2011;28(Suppl 6):1–18.
4. The BIG 1–98 Collaborative Group. Letrozole Therapy Alone or in Sequence with Tamoxifen in Women with Breast Cancer. N Engl J Med. 2009;361:766–76.
5. Cuzick J, Sestak I, Baum M, Buzdar A, Howell A, Dowsett M, Forbes JF, investigators AL: **Effect of anastrozole and tamoxifen as adjuvant treatment for early-stage breast cancer**: **10-year analysis of the ATAC trial**. *Lancet Oncology* 2010, **11**:1135–1141.
6. van de Velde CJ, Rea D, Seynaeve C, Putter H, Hasenburg A, Vannetzel JM, Paridaens R, Markopoulos C, Hozumi Y, Hille ETM, et al. Adjuvant tamoxifen and exemestane in early breast cancer (TEAM): a randomised phase 3 trial. Lancet. 2011;377:321–31.
7. Murphy CS, Pink JJ, Jordan VC. Characterization of a Receptor-negative, Hormone-nonresponsive Clone Derived from a T47D Human Breast Cancer Cell Line Kept under Estrogen-free Conditions. Can Res. 1990;50:7285–92.
8. Martin LA, Farmer I, Johnston SR, Ali S, Dowsett M. Elevated ERK1/ERK2/estrogen receptor cross-talk enhances estrogen-mediated signaling during long-term estrogen deprivation. Endocr Relat Cancer. 2005;12(Suppl 1):75–84.
9. Sabnis GJ, Jelovac D, Long B, Brodie A. The role of growth factor receptor pathways in human breast cancer cells adapted to long-term estrogen deprivation. Can Res. 2005;65:3903–10.
10. Santen RJ, Song RX, Masamura S, Yue W, Fan P, Sogon T, Hayashi S, Nakachi K, Eguchi H. Adaptation to estradiol deprivation causes up-regulation of growth factor pathways and hypersensitivity to estradiol in breast cancer cells. Adv Exp Med Biol. 2008;630:19–34.
11. Masri S, Phung S, Wang X, Wu X, Yuan YC, Wagman L, Chen S. Genome-wide analysis of aromatase inhibitor-resistant, tamoxifen-resistant, and long-term estrogen-deprived cells reveals a role for estrogen receptor. Cancer Res. 2008;68:4910–8.
12. Hanamura T, Hayashi SI. Overcoming aromatase inhibitor resistance in breast cancer: possible mechanisms and clinical applications. Breast Cancer. 2018;25:379–91.
13. Lewis JS, Meeke K, Osipo C, Ross EA, Kidawi N, Li T, Bell E, Chandel NS, Jordan VC. Intrinsic mechanism of estradiol-induced apoptosis in breast cancer cells resistant to estrogen deprivation. J Natl Cancer Inst. 2005;97:1746–59.
14. Ariazi EA, Cunliffe HE, Lewis-Wambi JS, Slifker MJ, Willis AL, Ramos P, Tapia C, Kim HR, Yerrum S, Sharma CG, et al. Estrogen induces apoptosis in estrogen deprivation-resistant breast cancer through

stress responses as identified by global gene expression across time. Proc Natl Acad Sci USA. 2011;108:18879–86.

15. Obiorah IE, Fan P, Jordan VC. Breast cancer cell apoptosis with phytoestrogens is dependent on an estrogen-deprived state. Cancer Prev Res (Phila). 2014;7:939–49.
16. Fan P, Tyagi AK, Agboke FA, Mathur R, Pokharel N, Jordan VC. Modulation of nuclear factor-kappa B activation by the endoplasmic reticulum stress sensor PERK to mediate estrogen-induced apoptosis in breast cancer cells. Cell Death Discovery. 2018;4:15.
17. Hosford SR, Shee K, Wells JD, Traphagen NA, Fields JL, Hampsch RA, Kettenbach AN, Demidenko E, Miller TW. Estrogen therapy induces an unfolded protein response to drive cell death in ER + breast cancer. Mol Oncol. 2019;13:1778–94.
18. Song RX-D, Mor G, Naftolin F, McPherson RA, Song J, Zhang Z, Yue W, Wang J. J. SR: Effect of Long-Term Estrogen Deprivation on Apoptotic Responses of Breast Cancer Cells to 17β-Estradiol. J Natl Cancer Inst. 2001;93:1714–23.
19. Kanaya N, Somlo G, Wu J, Frankel P, Kai M, Liu X, Wu SV, Nguyen D, Chan N, Hsieh MY, et al. Characterization of patient-derived tumor xenografts (PDXs) as models for estrogen receptor positive (ER + HER2- and ER + HER2+) breast cancers. Journal of Steroid Biochemistry Molecular Biology. 2017;170:65–74.
20. Sabnis GJ, Goloubeva OG, Kazi AA, Shah P, Brodie AH. HDAC inhibitor entinostat restores responsiveness of letrozole-resistant MCF-7Ca xenografts to aromatase inhibitors through modulation of Her-2. Mol Cancer Ther. 2013;12:2804–16.
21. Hennessy BT, Lu Y, Gonzalez-Angulo AM, Carey MS, Myhre S, Ju Z, Davies MA, Liu W, Coombes K, Meric-Bernstam F, et al. A Technical Assessment of the Utility of Reverse Phase Protein Arrays for the Study of the Functional Proteome in Non-microdissected Human Breast Cancers. Clin Proteomics. 2010;6:129–51.
22. Tirosh I, Izar B, Prakadan SM, Wadsworth MH, Treacy D, Trombetta JJ, Rotem A, Rodman C, Lian C, Murphy G, et al. Dissecting the multicellular ecosystem of metastatic melanoma by single-cell RNA-sEq. Science. 2016;352:189–96.
23. DeRose YS, Gligorich KM, Wang G, Georgelas A, Bowman P, Courdy SJ, Welm AL, Welm BE: **Patient-derived models of human breast cancer: protocols for in vitro and in vivo applications in tumor biology and translational medicine**. *Current Protocols in Pharmacology* 2013, Chap. 1**4**:Unit14 23.
24. Li S, Shen D, Shao J, Crowder R, Liu W, Prat A, He X, Liu S, Hoog J, Lu C, et al. Endocrine-therapy-resistant ESR1 variants revealed by genomic characterization of breast-cancer-derived xenografts. Cell Reports. 2013;4:1116–30.
25. Robinson DR, Wu YM, Vats P, Su F, Lonigro RJ, Cao X, Kalyana-Sundaram S, Wang R, Ning Y, Hodges L, et al. Activating ESR1 mutations in hormone-resistant metastatic breast cancer. Nat Genet. 2013;45:1446–51.
26. Toy W, Shen Y, Won H, Green B, Sakr RA, Will M, Li Z, Gala K, Fanning S, King TA, et al. ESR1 ligand-binding domain mutations in hormone-resistant breast cancer. Nat Genet. 2013;45:1439–45.

27. Raj GV, Sareddy GR, Ma S, Lee T-K, Viswanadhapalli S, Li R, Liu X, Murakami S, Chen C-C, Lee W-R, et al: **Estrogen receptor coregulator binding modulators (ERXs) effectively target estrogen receptor positive human breast cancers**. *eLife* 2017, **6**.
28. Clarke R, Leonessa F, Welch J, Skaar T. Cellular and Molecular Pharmacology of Antiestrogen Action and Resistance. Pharmacol Rev. 2001;53:25–71.
29. Hayashi S, Niwa T, Yamaguchi Y. Estrogen signaling pathway and its imaging in human breast cancer. Cancer Sci. 2009;100:1773–8.
30. Stossi F, Barnett DH, Frasor J, Komm B, Lyttle CR, Katzenellenbogen BS. Transcriptional profiling of estrogen-regulated gene expression via estrogen receptor (ER) alpha or ERbeta in human osteosarcoma cells: distinct and common target genes for these receptors. Endocrinology. 2004;145:3473–86.
31. Lebedeva IV, Su ZZ, Chang Y, Kitada S, Reed JC, Fisher PB. The cancer growth suppressing gene mda-7 induces apoptosis selectively in human melanoma cells. Oncogene. 2002;21:708–18.
32. Sauane M, Gopalkrishnan RV, Sarkar D, Su ZZ, Lebedeva IV, Dent P, Pestka S, Fisher PB. MDA-7/IL-24: novel cancer growth suppressing and apoptosis inducing cytokine. Cytokine Growth Factor Rev. 2003;14:35–51.
33. Marquez-Jurado S, Diaz-Colunga J, das Neves RP, Martinez-Lorente A, Almazan F, Guantes R, Iborra FJ. Mitochondrial levels determine variability in cell death by modulating apoptotic gene expression. Nat Commun. 2018;9:389.
34. Khongthong P, Roseweir AK, Edwards J. The NF-KB pathway and endocrine therapy resistance in breast cancer. Endocr Relat Cancer. 2019;26:R369–80.
35. Liao Z, Chua D, Tan NS. Reactive oxygen species: a volatile driver of field cancerization and metastasis. Mol Cancer. 2019;18:65.
36. Assi M. The differential role of reactive oxygen species in early and late stages of cancer. Am J Physiol Regul Integr Comp Physiol. 2017;313:R646–53.
37. Cutano V, Giorgio ED, Minisini M, Picco R, Dalla E, Brancolini C. HDAC7-mediated control of tumour microenvironment maintains proliferative and stemness competence of human mammary epithelial cells. Mol Oncol. 2019;13:1651–68.
38. Cao SS, Kaufman RJ. Endoplasmic reticulum stress and oxidative stress in cell fate decision and human disease. Antioxid Redox Signal. 2014;21:396–413.
39. Lebedeva IV, Su Z-Z, Sarkar D, Kitada S, Dent P, Waxman S, Reed JC, Fisher PB: **Melanoma Differentiation Associated Gene-7, mda-7/Interleukin-24, Induces Apoptosis in Prostate Cancer Cells by Promoting Mitochondrial Dysfunction and Inducing Reactive Oxygen Species**. *Cancer Research* 2003, **63**:8138–8144.
40. Haddow A, Watkinson JM, Paterson E, Koller PC. Influence of synthetic oestrogens on advanced malignant disease. BMJ. 1944;2:393–8.
41. Ingle JN, Ahmann DL, Green SJ, Edmonson JH, Bisel HF, Kvols LK, Nichols WC, Creagan ET, Hahn RG, Rubin J, Frytak S. Randomized clinical trial of diethylstilbestrol versus tamoxifen in postmenopausal

women with advanced breast cancer. The New England Journal of Medicine. 1981;304:16–21.

42. Beex L, Pieters G, Smals A, Koenders A, Benraad T, Kloppenborg P. Tamoxifen versus ethinyl estradiol in the treatment of postmenopausal women with advanced breast cancer. Cancer Treat Rep. 1981;65:179–85.
43. Heuson JC, Engelsman E, Blonk-Van Der Wijst J, Maass H, Drochmans A, Michel J, Nowakowski H, Gorins A. Comparative trial of nafoxidine and ethinyloestradiol in advanced breast cancer: an E.O.R.T.C. study. British medical journal. 1975;2:711–3.
44. Lønning P, Taylor P, Anker G, Iddon J, Wie L, Jørgensen L-M, Mella O, Howell A. High-dose estrogen treatment in postmenopausal breast cancer patients heavily exposed to endocrine therapy. Breast Cancer Res Treat. 2001;67:111–6.
45. Agrawal A, Robertson JF, Cheung KL. Efficacy and tolerability of high dose "ethinylestradiol" in post-menopausal advanced breast cancer patients heavily pre-treated with endocrine agents. World Journal of Surgical Oncology. 2006;4:44.
46. Ellis MJ, Gao F, Dehdashti F, Jeffe DB, Marcom PK, Carey LA, Dickler MN, Silverman P, Fleming GF, Kommareddy A, et al. Lower-dose vs high-dose oral estradiol therapy of hormone receptor-positive, aromatase inhibitor-resistant advanced breast cancer: a phase 2 randomized study. JAMA. 2009;302:774–80.
47. Iwase H, Yamamoto Y, Yamamoto-Ibusuki M, Murakami KI, Okumura Y, Tomita S, Inao T, Honda Y, Omoto Y, Iyama KI. Ethinylestradiol is beneficial for postmenopausal patients with heavily pre-treated metastatic breast cancer after prior aromatase inhibitor treatment: a prospective study. Br J Cancer. 2013;109:1537–42.
48. Chalasani P, Stopeck A, Clarke K, Livingston R. A pilot study of estradiol followed by exemestane for reversing endocrine resistance in postmenopausal women with hormone receptor-positive metastatic breast cancer. Oncologist. 2014;19:1127–8.
49. Zucchini G, Armstrong AC, Wardley AM, Wilson G, Misra V, Seif M, Ryder WD, Cope J, Blowers E, Howell A, et al. A phase II trial of low-dose estradiol in postmenopausal women with advanced breast cancer and acquired resistance to aromatase inhibition. Eur J Cancer. 2015;51:2725–31.

Figures

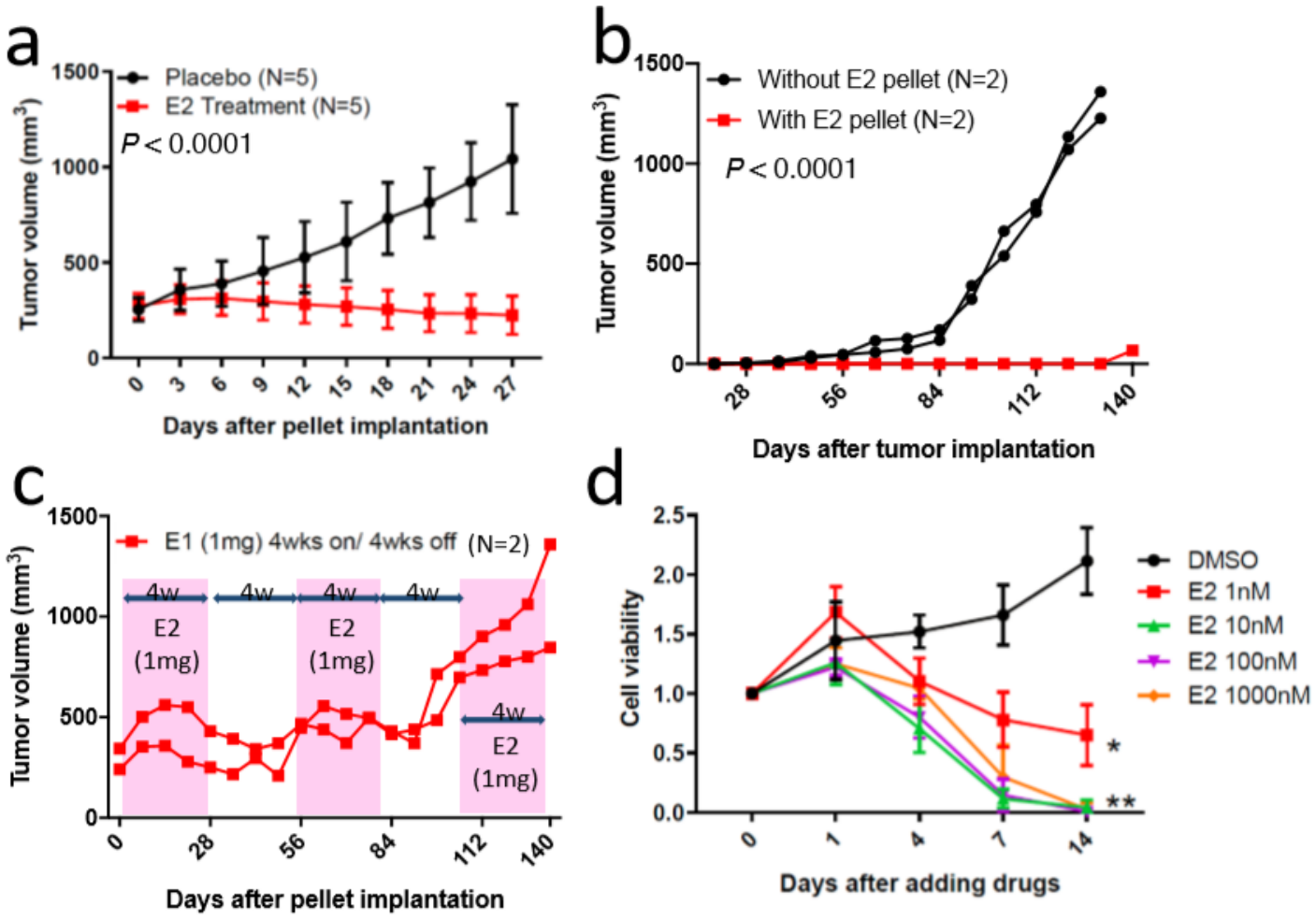

Figure 1

E2 inhibited the growth of GS3 both in vivo and in vitro. (a) Tumor growth curve of GS3-PDX with E2 (1 mg) or placebo treatment for 28 days. Pellets were implanted in mice after tumor volume reached approximately 200mm3. (b) Tumor growth curves of GS3-PDX with/without E2 (1 mg). Tumors and pellets were implanted at the same time. (c) Tumor growth curves of intermittent E2 (1 mg) treatment which was performed every 28 days (E2 pellet on/off every 4 weeks, three times) after tumor volume reached approximately 200mm3. (d) Cell viability of 104 organoids (isolated from GS3 tumor) treated with varying concentrations of E2 in vitro (*P = 0.000025, **P < 0.000001 on Day 14). Error bars represent SEM.

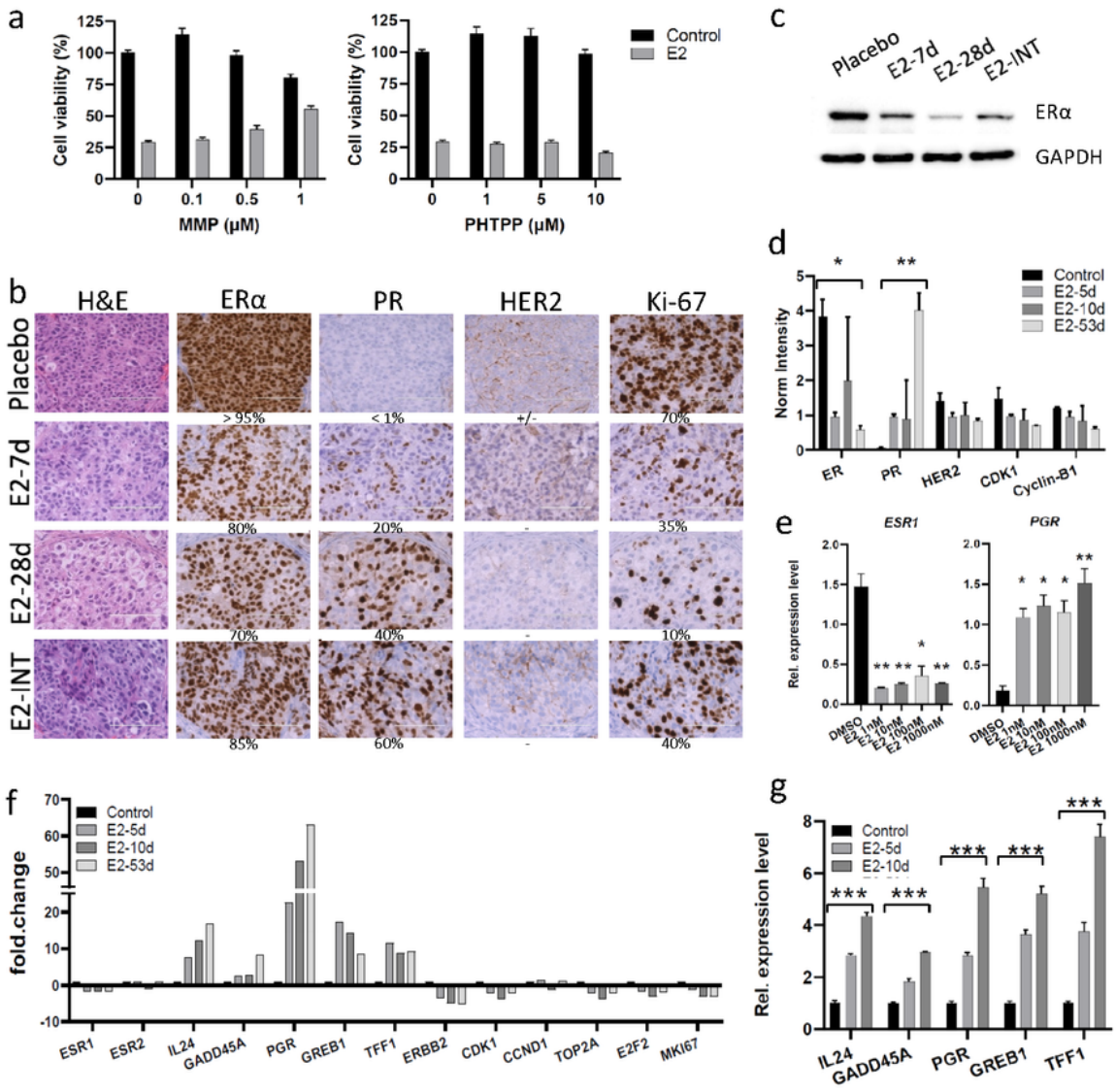

Figure 2

E2 suppressed the expression of ERα and cell cycle proliferation genes in GS3. (a) Cell viability of organoids (isolated from GS3 tumor) co-treated with E2 and ERα antagonist (MPP) or ERβ antagonist (PHTPP) in vitro. (b) Hematoxylin and eosin staining and immunohistochemistry of GS3 tumors treated with placebo, 7-day E2, 28-day E2 and intermittent E2. Scale bar represents 100 μm. (c) ERα expression of GS3 tumors treated with placebo, 7-day E2, 28-day E2 and intermittent E2 by western blotting. (d) Protein

expression levels of GS3 tumors treated with 5-, 10-, 53-day E2, and control samples as determined by reverse phase protein array analysis (*P < 0.05, **P < 0.01). (e) ESR1 and PGR expression levels of GS3-organoids treated with varying concentrations of E2 in vitro (*P < 0.05, **P < 0.01). (f) Fold changes of gene expression in GS3 tumors treated with 5-, 10-, 53-day E2, and control sample as determined by Bulk RNAseq. Each treatment included two samples. (g) Gene expression levels of GS3-organoids isolated from GS3 tumors with 5- and 10-day E2, and control sample (***P < 0.0001). E2-7d, E2 treatment for 7 days; E2-28d, E2 treatment for 28 days; E2-INT, intermittent E2 treatment. Error bars represent SEM.

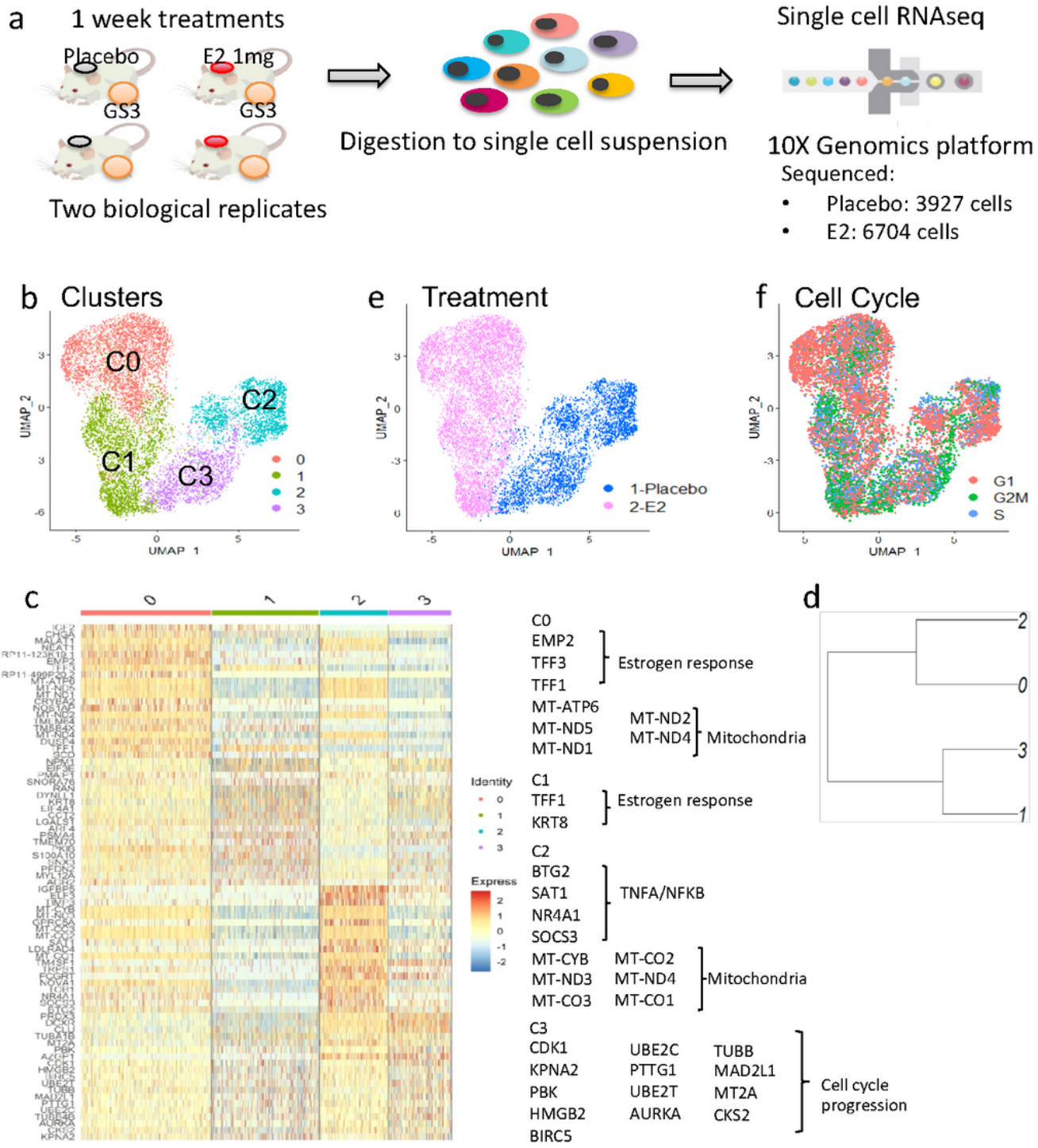

Figure 3

Effects of E2 on GS3 were studied by scRNAseq. (a) Overview of scRNAseq approach using PDX tumors. (b) UMAP of cells from both placebo- and E2-treated GS3-PDX. There were four major clusters in GS3. (c) Heat map using the top 20 differentially expressed genes. (d) Dendogram showing cluster relationship to other clusters based on gene expression data. (e) UMAP of cells color-coded according to treatments. (f) UMAP of cells color-coded according to cell cycle phases.

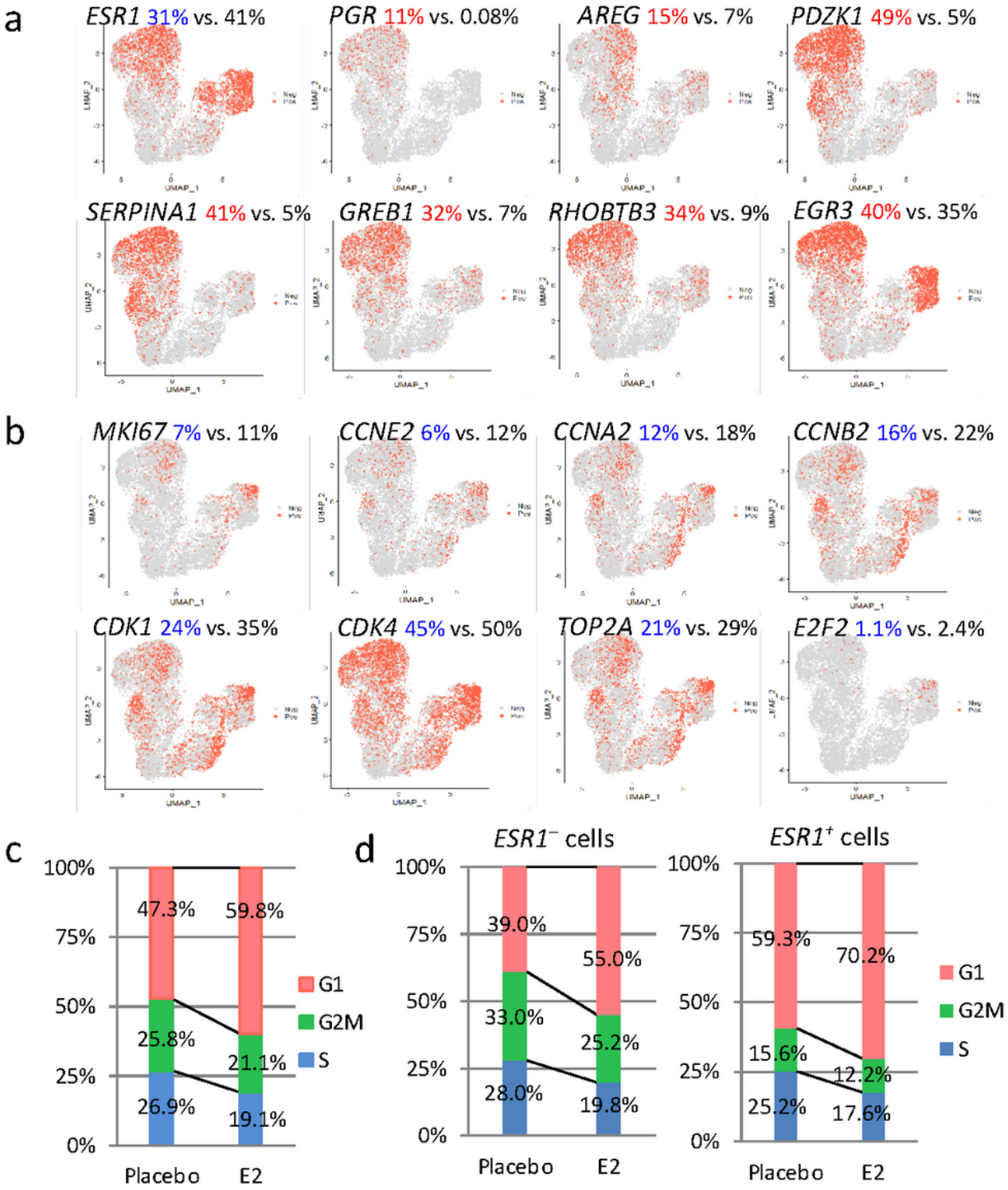

Figure 4

Gene expression comparison of E2-treated cells versus placebo-treated cells. (a) Selected feature plots of cells expressing ESR1 and ER regulated genes in UMAP. (b) Selected feature plots of cells expressing cell cycle progression genes in UMAP. (c) Distribution of cells staying at the G1, S, or G2M phase in all cells. (d) Distribution of cells staying at the G1, S, or G2M phase in ESR1+ cells and ESR1– cells.

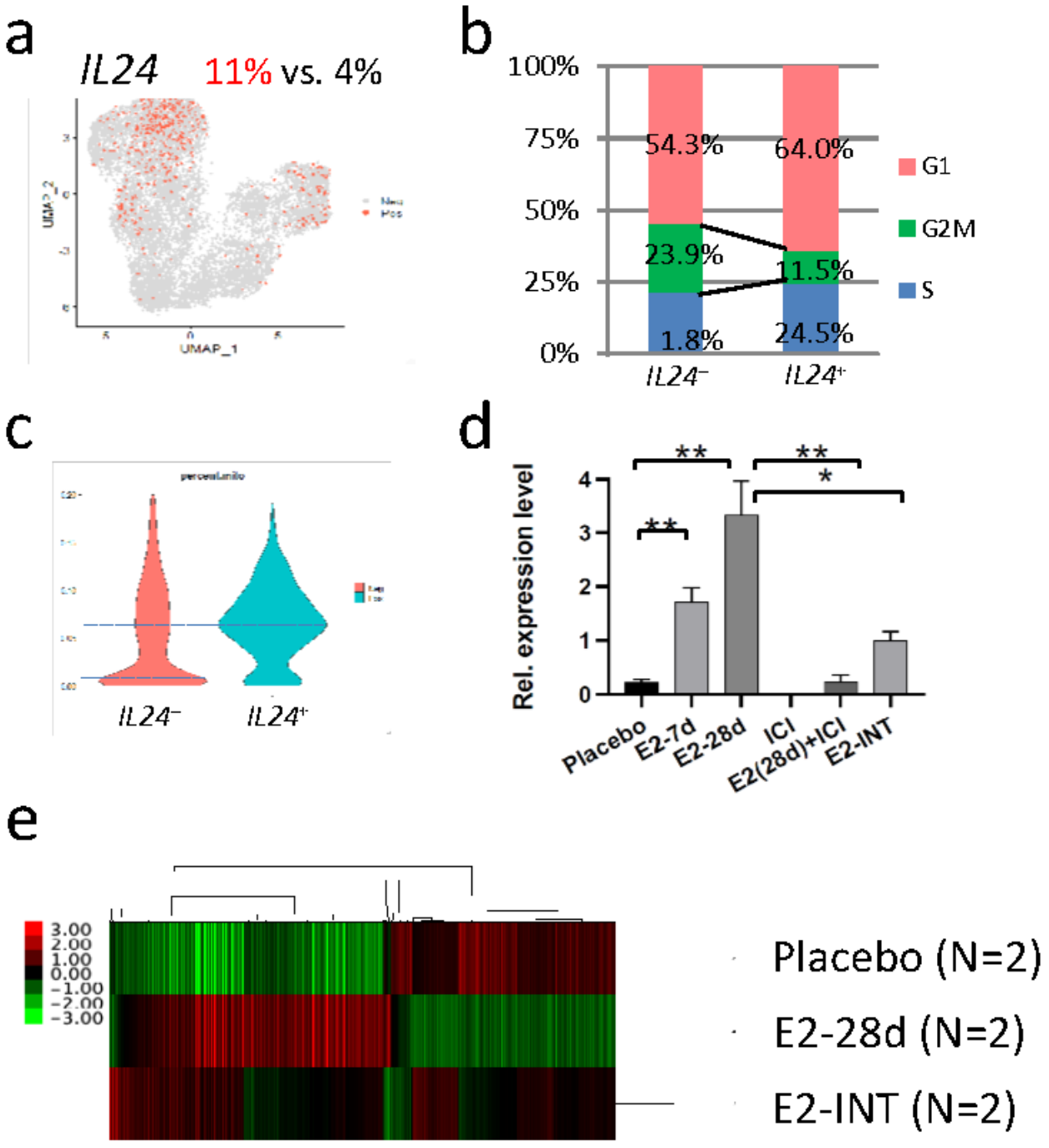

Figure 5

Percentage of IL24+ cells increased by E2 treatment through ERα. (a) Feature plot of cells expressing IL24 in UMAP from scRNAseq. (b) Distribution of cells staying at the G1, S, or G2M phase in IL24+ cells or IL24− cells from scRNAseq. (c) Violin plots of the percentage of mitochondrial genes in IL24+ cells and IL24− cells from scRNAseq. (d) IL24 expression levels in GS3 tumors with different treatments including E2 and ICI (*P < 0.05, **P < 0.01). (e) Hierarchical clustering using 1,312 differentially expressed genes from bulk RNAseq. Error bars represent SEM. E2-7d, E2 treatment for 7 days; E2-28d, E2 treatment for 28 days; ICI, ICI treatment for 28 days (once weekly, four times); E2-INT, intermittent E2 treatment.

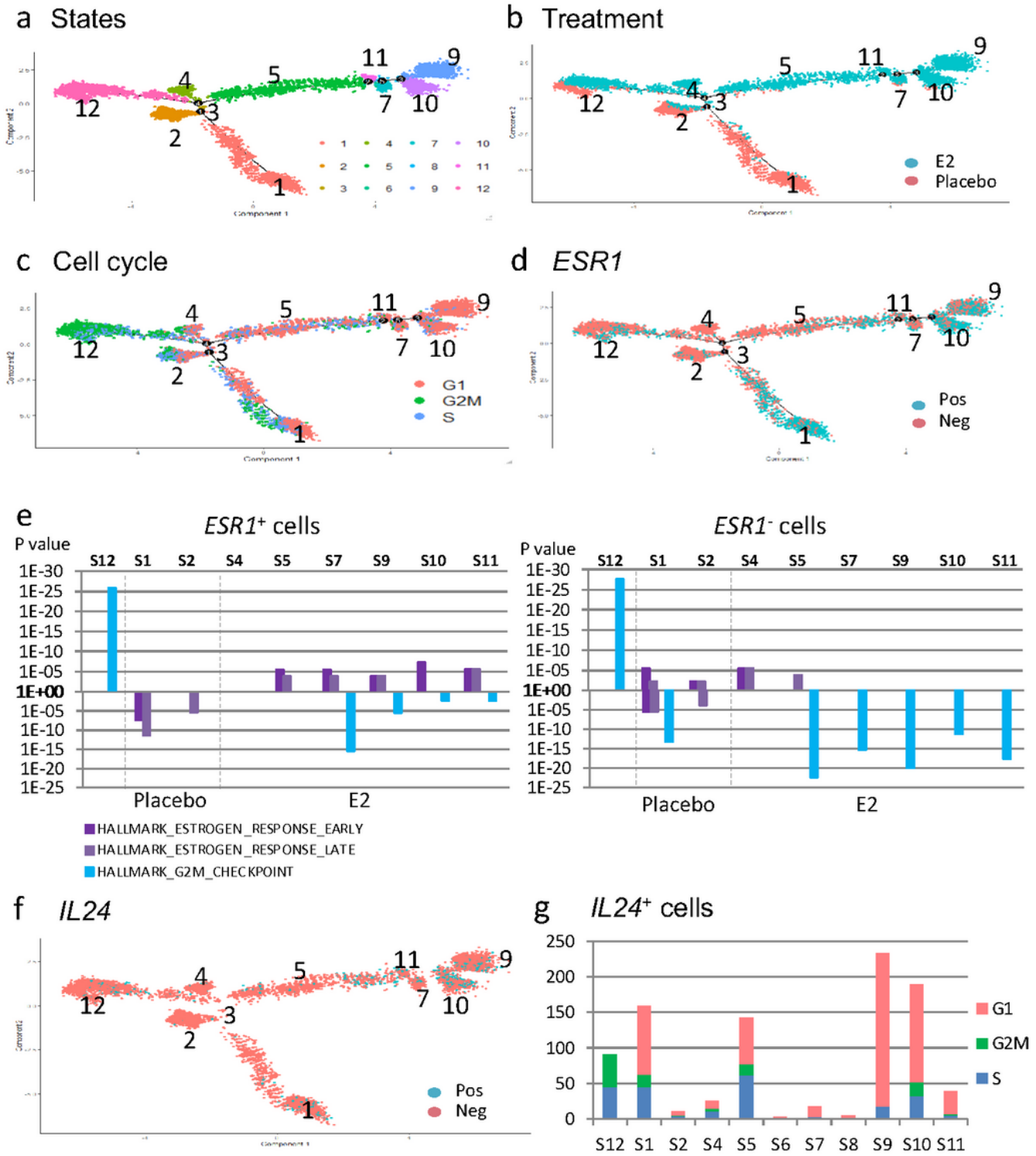

Figure 6

Predication of the transitions between placebo-treated cells and E2-treated cells by trajectory analysis. (a) Cells color-coded according to states in the trajectory Monocle reconstructed. (b) Cells color-coded according to treatments in the trajectory Monocle reconstructed. (c) Cells color-coded according to cell cycle phases in the trajectory Monocle reconstructed. (d) Feature plot of ESR1+ cells in the trajectory Monocle reconstructed. (e) Hallmark gene sets analysis of ESR1+ cells and ESR1– cells using top/bottom 20 differentially expressed genes in each cluster. (f) Feature plot of IL24+ cells in the trajectory Monocle reconstructed. (g) The number of IL24+ cells in each state.

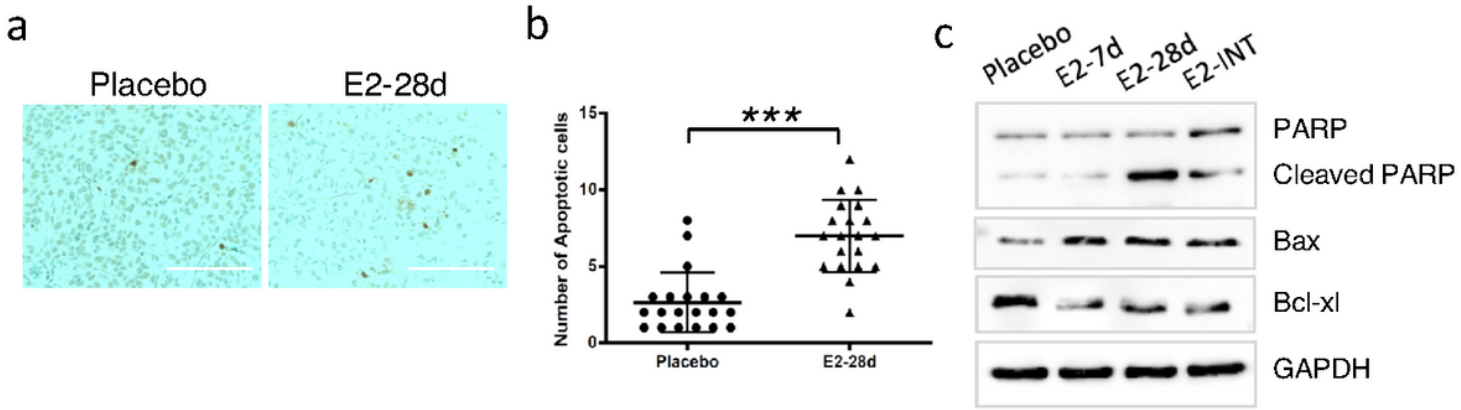

Figure 7

Long term E2 treatment induced apoptosis in GS3. (a) Apoptotic cells staining of GS3 tumors treated with placebo or 28-day E2. Scale bar represents 100 μm. (b) Apoptotic cell count of placebo and 28-day E2 treatment samples (each N = 5, pick up 5 spots randomly, ***P < 0.0001). Error bars represent SEM. (c) Expression of apoptosis-associated proteins of GS3 tumors treated with placebo, 7-day E2, 28-day E2 and intermittent E2 by western blotting. E2-7d, E2 treatment for 7 days; E2-28d, E2 treatment for 28 days; E2-INT, intermittent E2 treatment.

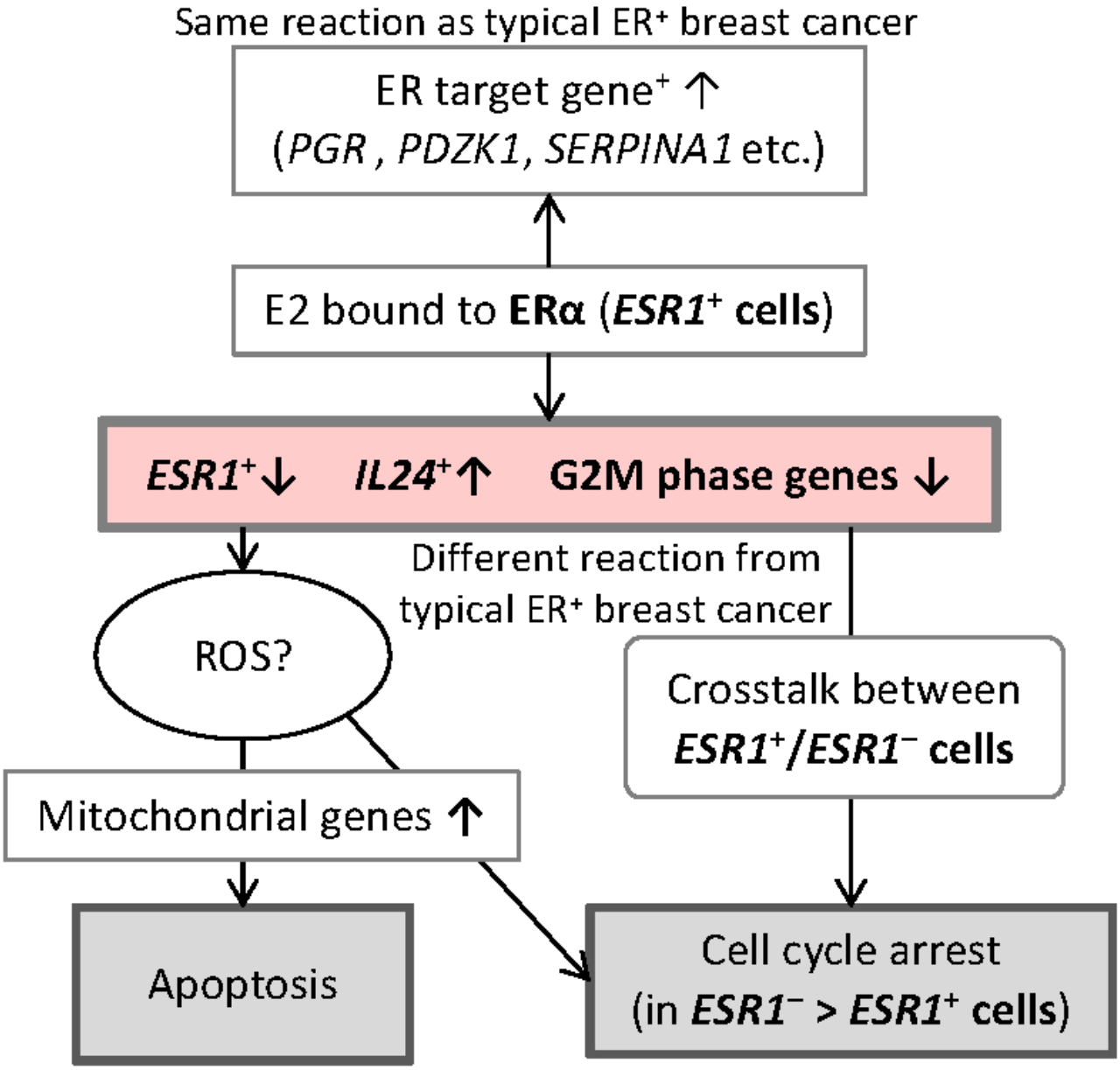

Figure 8

proposed mechanism of E2 induced tumor regression in GS3. After E2 treatment, the number of ER target gene-positive cells increased as typical ER+ breast cancer. However, in GS3, the number of ESR1+ cells and G2M phase cells decreased following the E2 treatment. More importantly, E2 increased the percentage of cells expressing IL24, which was known as a tumor suppressor gene. As a result of IL24 induced by E2 in GS3, the ROS pathway was upregulated, and then the apoptotic pathway was activated.

Unexpectedly, E2 also induced the expression of estrogen-regulated genes and cell cycle arrest in ESR1– cells. This finding could suggest a crosstalk between ESR1+ cells and ESR1– cells in this ER+ tumor.

Supplementary Files

This is a list of supplementary files associated with this preprint. Click to download.

- Suppldata.pdf